PLANT SCIENCES

# Resurrection of plant disease resistance proteins via helper NLR bioengineering

**Mauricio P. Contreras[1], Hsuan Pai[1], Muniyandi Selvaraj[1], AmirAli Toghani[1], David M. Lawson[2], Yasin Tumtas[3], Cian Duggan[3], Enoch Lok Him Yuen[3], Clare E. M. Stevenson[2], Adeline Harant[1], Abbas Maqbool[2], Chih-Hang Wu[4], Tolga O. Bozkurt[3], Sophien Kamoun[1]*, Lida Derevnina[1]†***



**Parasites counteract host immunity by suppressing helper nucleotide binding and leucine-rich repeat (NLR) proteins that function as central nodes in immune receptor networks. Understanding the mechanisms of immunosuppression can lead to strategies for bioengineering disease resistance. Here, we show that a cyst nematode virulence effector binds and inhibits oligomerization of the helper NLR protein NRC2 by physically preventing intramolecular rearrangements required for activation. An amino acid polymorphism at the binding interface between NRC2 and the inhibitor is sufficient for this helper NLR to evade immune suppression, thereby restoring the activity of multiple disease resistance genes. This points to a potential strategy for resurrecting disease resistance in crop genomes.**

## INTRODUCTION

The nucleotide binding and leucine-rich repeat (NLR) class of intracellular immune receptors is an important component of innate immunity in plants and animals. They mediate intracellular recognition of pathogens and subsequently initiate an array of immune responses to counteract infection (*1*, *2*). NLRs can be activated by pathogen-secreted virulence proteins, termed effectors, which pathogens deliver into host cells to modulate host physiology (*2*). A hallmark of plant and animal NLR activation is their oligomerization into higher-order immune complexes termed resistosomes or inflammasomes, respectively (*3*–*9*). These complexes initiate immune signaling via diverse mechanisms, often leading to a form of programmed cell death, termed hypersensitive response (HR) in plants or pyroptosis in animals (*10*, *11*). Recent studies have reported NLR-like proteins mediating antiviral immunity and programmed cell death in prokaryotes via mechanisms analogous to those found in eukaryotic NLRs, suggesting that this is a conserved defense mechanism across all three domains of life (*12*). Pathogen effectors can act both as triggers and suppressors of NLR-mediated immunity (*13*). In some cases, adapted pathogens deploy effectors that directly or indirectly interfere with NLR signaling to suppress immune activation (*12*, *14*–*17*). However, the exact biochemical mechanisms by which pathogen effectors compromise NLR-mediated immunity to promote disease remain largely unknown. Moreover, whereas multiple strategies to bioengineer effector recognition specificities in NLRs have been proposed in recent years (*18*), approaches to mitigate the impact of effector-mediated immune suppression of NLRs are lacking.

NLRs belong to the signal adenosine triphosphatases (ATPases) with numerous domains (STAND) superfamily. They typically exhibit a tripartite domain architecture consisting of an N-terminal signaling domain, a central nucleotide binding domain, and C-terminal superstructure forming repeats (*2*). The central domain, termed NB-ARC (nucleotide binding adaptor shared by APAF-1, plant R proteins, and CED-4) in plant NLRs, is a hallmark of this protein family and plays a key role as a molecular switch, mediating conformational changes required for activation. NB-ARC domains consist of a nucleotide binding domain (NB), a helical domain (HD1), and a winged helix domain (WHD) (*2*, *19*). Diverse NLR activation and signaling strategies are found in nature. In some cases, one NLR protein, termed a singleton, can mediate both elicitor perception and subsequent immune signaling (*20*). However, some NLRs can function as receptor pairs or, in higher-order configurations, termed immune receptor networks (*13*, *21*). In these cases, one NLR acts as a pathogen sensor, requiring a second helper NLR to initiate immune signaling. Such is the case in the solanaceous NRC immune receptor network, which is composed of multiple sensor NLRs that require an array of downstream helper NLRs termed NRCs (NLRs required for cell death) to successfully initiate immune signaling. Upon perception of their cognate effectors, sensors in this network activate oligomerization of their downstream NRC helpers into a putative NRC resistosome, without stably forming part of the mature complex. This has been termed the activation and release model (*4*). The NRC network can encompass up to half of the NLRome in some solanaceous plant species and plays a key role in mediating immunity against a variety of plant pathogens including oomycetes, bacteria, viruses, nematodes, and insects (*15*, *21*).

Plant and metazoan parasites have evolved effectors that interfere with host NLR signaling to promote disease. Parasite effectors can suppress NLR-mediated immunity indirectly by interfering with host proteins that act downstream of NLR signaling (*15*, *17*, *22*, *23*) or directly by interacting with NLRs to inhibit their functions (*15*, *16*, *24*). One such example is the potato cyst nematode (*Globodera rostochiensis*) effector, SPRYSEC15 (SS15), which can suppress signaling mediated by *Nicotiana benthamiana* helper NLRs NRC2 and NRC3 and tomato (*Solanum lycopersicum*) helper NLR NRC1, by binding to their central NB-ARC domains.

[1]The Sainsbury Laboratory, University of East Anglia, Norwich, UK. [2]Department of Biochemistry and Metabolism, John Innes Centre, Norwich, UK. [3]Department of Life Sciences, Imperial College, London, UK. [4]Institute of Plant and Microbial Biology, Academia Sinica, Taipei, Taiwan.
*Corresponding author. Email: sophien.kamoun@tsl.ac.uk (S.K.); ld645@cam.ac.uk (L.D.)
†Present address: Crop Science Centre, Department of Plant Sciences, University of Cambridge, Cambridge, UK.

In contrast, another *N. benthamiana* helper NLR NRC4, a paralog of NRC2/3, cannot be suppressed by SS15 (Fig. 1A and fig. S1A) (*15*). In this study, we reasoned that mapping the binding interface between SS15 and its target helper NLRs combined with leveraging NRC4 resilience to inhibition would enable us to bioengineer NLR variants that evade pathogen suppression, therefore resurrecting the immune signaling activity of upstream sensors in the NRC network.

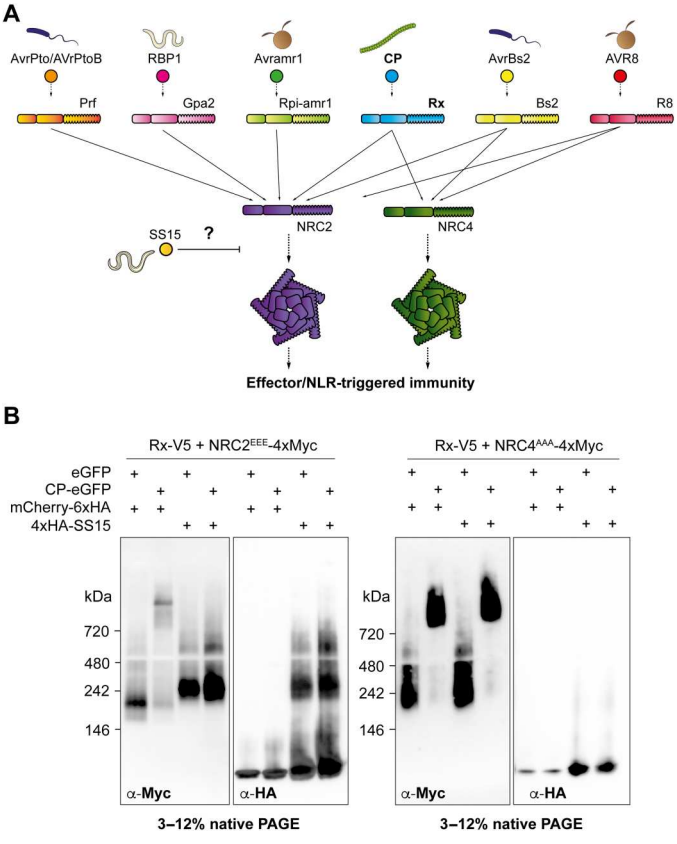


**Fig. 1. SS15 directly inhibits NRC2 but not NRC4 oligomerization.** (**A**) Schematic representation of the NRC immune receptor network, consisting of multiple sensor NLRs and their downstream helper NLRs, NRC2 and NRC4 (in purple and green, respectively). Potato virus X (PVX) capsid protein (CP) and Rx are in boldface as they are used for most of the experiments in this study. Effector-triggered activation of a sensor leads to downstream helper oligomerization and resistosome formation. The *G. rostochiensis* effector SS15 (in yellow) can directly bind to the NB-ARC domain of NRC2 but not NRC4, thereby inhibiting signaling by directly binding to the NB-ARC domain of this helper NLR. (**B**) Blue native polyacrylamide gel electrophoresis (BN-PAGE) assays with inactive and activated Rx together with NRC2 or NRC4, in the absence or presence of SS15. C-terminally V5-tagged Rx and C-terminally 4xMyc-tagged NRC2$^{EEE}$ or NRC4$^{AAA}$ were coexpressed with either free green fluorescent protein (GFP) or C-terminally GFP-tagged PVX CP. These effector-sensor-helper combinations were coinfiltrated together with a 6xHA-mCherry fusion protein or with N-terminally 6xHA-tagged SS15. Total protein extracts were run in parallel on native and denaturing PAGE assays and immunoblotted with the appropriate antisera labeled below. Approximate molecular weights (in kilodalton) of the proteins are shown on the left. Corresponding SDS-PAGE assays can be found in fig. S1. The experiment was repeated three times with similar results.

## RESULTS

### SS15 blocks NRC2 but not NRC4 oligomerization and resistosome formation

First, we investigated how SS15 binding to NRC2 prevents immune signaling, notably whether SS15 prevents oligomerization of NRC following sensor NLR activation. To test this hypothesis, we transiently coexpressed NRC2 or NRC4 with their upstream sensor NLR Rx and the effector SS15 in leaves of *nrc2/3/4* CRISPR knockout (KO) *N. benthamiana* plants and leveraged previously established blue native polyacrylamide gel electrophoresis (BN-PAGE)–based readouts for NRC resistosome formation (*4*). For biochemical analyses, we used previously described NRC2 and NRC4 variants with mutations in their N-terminal MADA motifs (NRC2$^{EEE}$ and NRC4$^{AAA}$, respectively), which abolish cell death induction without compromising receptor activation, oligomerization, or localization (*4*, *25*, *26*). We activated the sensor helper Rx-NRC system by coexpressing the potato virus X (PVX) capsid protein (CP) fused to green fluorescent protein (GFP) or free GFP as an inactive control. In the absence of SS15, both NRC2 and NRC4 oligomerize upon effector-triggered activation mediated by their upstream sensor Rx. However, when SS15 is present, Rx/CP-activated NRC2 is unable to oligomerize and appears as a band of ~240 kDa, which co-migrates with SS15. Inactive NRC2 coexpressed with SS15 also migrates as a band of ~240 kDa, which is slower-migrating relative to inactive NRC2 in the absence of SS15, indicative of in vivo NRC2-SS15 complex formation (Fig. 1B and fig. S1). We also observed that SS15 coexpression not only blocks NRC2 oligomerization but also prevents the previously reported shift of NRC2 from cytoplasm to plasma membrane (PM) as well as the formation of NRC2 PM-associated puncta upon Rx/CP activation (fig. S2) (*4*). In contrast, NRC4 oligomerization is not affected in the presence of SS15, which is in line with previous findings that NRC4 immune signaling is not suppressed by SS15 (*15*). We conclude that SS15 can suppress immune signaling by acting as a direct proteinaceous inhibitor of NRC2, but not NRC4, by directly binding to its NB-ARC domain to block the formation of a signal-competent oligomeric resistosome.

### SS15 binds and immobilizes a critical "hinge" in the NB-ARC domain

Given that NRC4 retains the capacity to oligomerize in the presence of SS15, we leveraged this differential SS15 sensitivity between NRC2 and NRC4 to identify the domain that determines SS15 association and inhibition. We generated a series of NRC2-NRC4 chimeric proteins (Fig. 2, A and B, and fig. S3), which we subsequently assayed for SS15 association via in planta co-immunoprecipitation. We identified one chimeric variant of NRC4, carrying the HD1-1 region of NRC2 (NRC4$^{2HD1\text{-}1}$), which gains association to SS15 (Fig. 2C). Unlike NRC4, NRC4$^{2HD1\text{-}1}$ is susceptible to inhibition by SS15 and is unable to oligomerize and trigger cell death in the presence of SS15 (Fig. 2, D and E, and figs. S3 and S4). We conclude that the HD1-1 region is important for association to SS15 and for the effector to directly inhibit NRC oligomerization and programmed cell death.

To further define the interface between SS15 and NRC proteins, we attempted to crystallize SS15 in complex with the NB-ARC domain of several NRC proteins. We obtained crystals of SS15 in complex with the NB-ARC domain of SlNRC1, a tomato NRC

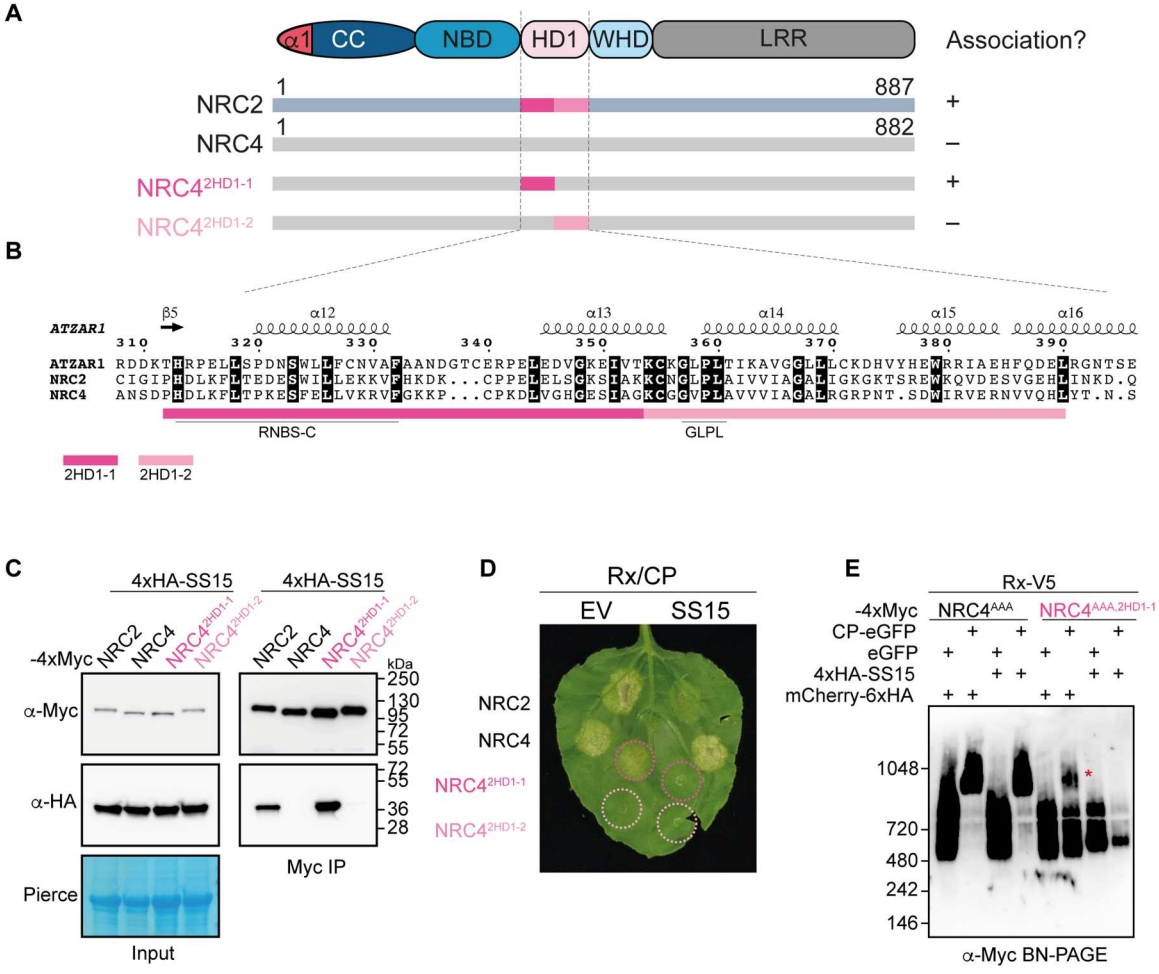


**Fig. 2. The HD1-1 region of NRC NB-ARC domain determines sensitivity to SS15.** (**A**) Schematic representation of the NRC domain architecture, highlighting regions within the NB-ARC domain swapped between NRC2-NRC4 chimeric proteins. Association (+) or lack thereof (–) between these NLR immune receptors and SS15 determined by in planta co-immunoprecipitation (Co-IP) is detailed on the right. (**B**) Amino acid sequence alignment of the HD1 region of the NB-ARC domains of AtZAR1, NRC2, and NRC4. Predicted secondary structure is shown above. Well-characterized motifs within this region are underlined below. (**C**) Co-IP assays between SS15 and chimeric NRC2-NRC4 variants. C-terminally 4xMyc-tagged NRC proteins were coexpressed with N-terminally 4xHA-SS15. IPs were performed with agarose beads conjugated to Myc antibodies (Myc IP). Total protein extracts were immunoblotted with the antisera labeled on the left. Approximate molecular weights (in kilodalton) of the proteins are shown on the right. Rubisco loading control was carried out using Ponceau stain (PS). The experiment was repeated three times with similar results. (**D**) Photo of representative leaves from *N. benthamiana nrc2/3/4* KO plants showing HR after coexpression of Rx/PVX CP with NRC2/NRC4 and the two NRC2-NRC4 chimeras. Combination shown were coexpressed with mCherry-6xHA (EV) or 4xHA-SS15. Three biological replicates with at least six technical replicates each are shown. Quantitative analyses of the HR phenotypes are found in fig. S4. (**E**) BN-PAGE assay with inactive and activated Rx with NRC4 or an NRC2-NRC4 chimeric protein in the absence or presence of SS15. Effector-sensor-helper combinations shown were coinfiltrated together with mCherry-6xHA or with 4xHA-SS15. Total protein extracts were run in parallel on native and denaturing PAGE and immunoblotted with the antisera labeled on the left. SDS-PAGE blots are found in fig. S3. Approximate molecular weights (in kilodalton) of the proteins are shown on the left. The experiment was repeated three times with similar results.

that is inhibited by the nematode effector. Because purification and crystallization trials of SS15 in complex with $NRC2^{NB\text{-}ARC}$ and $NRC3^{NB\text{-}ARC}$ were unsuccessful, we moved forward with the $SlNRC1^{NB\text{-}ARC}$-SS15 crystals. We subsequently solved the structure using x-ray diffraction data collected to 4.5-Å resolution (Fig. 3A, fig. S5, and table S3), which allowed us to determine that SS15 binds to a loop in the HD1-1 region of NRCs that connects the NB domain to the HD1 and WHD domains. This provides orthogonal evidence that the SS15-NRC interactions are mediated by this region as shown with the chimera experiments (Fig. 2). This loop was previously shown to act as a "hinge," allowing the NB domain to rotate relative to the HD1 and WHD domains following activation (fig. S5 and movie S1) (*27*). We propose that SS15 prevents conformational changes that are critical for NLR activation by binding and immobilizing the NB-HD1 hinge.

## Single amino acid variants of NRC2 evade suppression by SS15

Given that SS15 suppresses cell death induction mediated by SlNRC1, NRC2, and NRC3 but not NRC4 or other well-characterized NLRs such as ZAR1 (fig. S1) (*15*), we leveraged the high degree of conservation that is characteristic of plant NB-ARC domains to narrow down residues within the binding interface that underpin this interaction. We shortlisted residues within the HD1-1 region

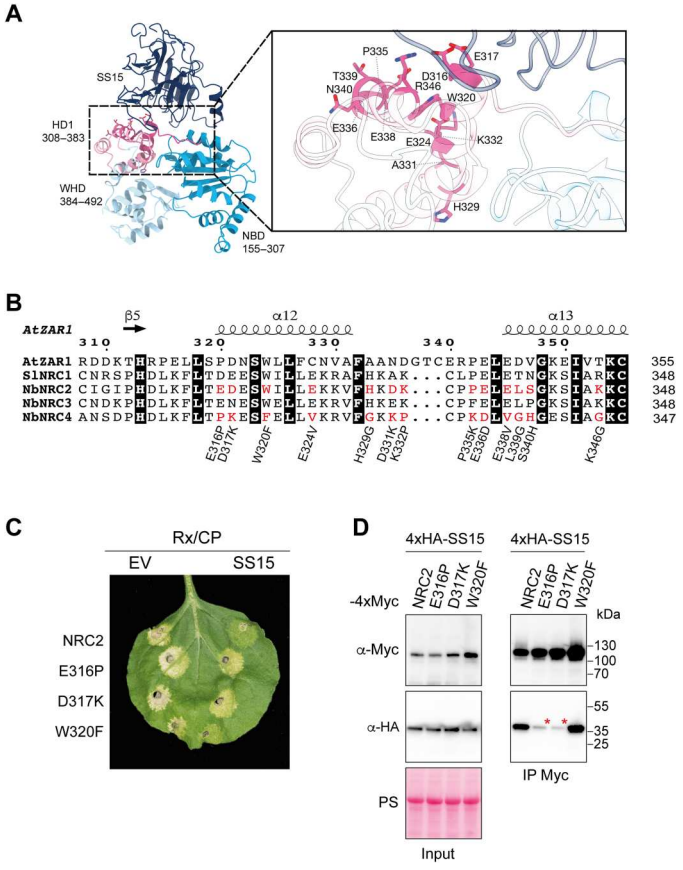


**Fig. 3. SS15-NRC binding interface enables bioengineering NRC2 variants that evade suppression.** (**A**) Crystal structure of the SS15-SlNRC1$^{NB-ARC}$ complex. The NB, HD1, and WHD domains of SlNRC1$^{NB-ARC}$ are shown in cyan, pale blue, and magenta, respectively; SS15 is in dark blue. The inset displays a close-up image of the SS15-SlNRC1$^{NB-ARC}$ HD1 domain interface, with the residues corresponding to those selected for mutagenesis in NRC2 highlighted in stick representation. (**B**) Alignment of the HD1-1 region of AtZAR1, SlNRC1, NRC2, NRC3, and NRC4. Candidate residues (highlighted in red) were shortlisted on the basis of the interface identified in the co-crystal structure of SS15 and the SlNRC1 NB-ARC domain, as well as being conserved in SlNRC1, NRC2, and NRC3 but not NRC4 and AtZAR1. Thirteen NRC2 variants were generated by mutating individual candidate positions to the corresponding amino acid in NRC4 (detailed underneath the alignment). (**C**) Photo of representative leaves from *N. benthamiana nrc2/3/4* KO plants showing HR after coexpression of Rx and PVX CP with NRC2, or different NRC2 variants generated. All proteins were coexpressed with a free mCherry-6xHA fusion protein (EV) or with N-terminally 4xHA-tagged SS15. The experiment consisted of three biological replicates. See fig. S7 quantitative analysis of HR phenotypes. (**D**) Co-IP assays between SS15 and NRC2 variants. C-terminally 4xMyc-tagged NRC2 variants were transiently coexpressed with N-terminally 4xHA-tagged SS15. IPs were performed with agarose beads conjugated to Myc antibodies (Myc IP). While only data for E316P, D317K, and W320F NRC2 variants are shown, additional variants were also tested and can be found in fig S6. Total protein extracts were immunoblotted with appropriate antisera labeled on the left. Approximate molecular weights (in kilodalton) of the proteins are shown on the right. Rubisco loading control was carried out using PS. The experiment was repeated three times with similar results.

that are similar in SlNRC1, NRC2, and NRC3 but different in NRC4 or AtZAR1 (Fig. 3B). Combining information from the cocrystal structure and the alignments allowed us to select 13 candidate residues to test by mutagenesis in NRC2 (Fig. 3B). We mutated each of these residues to the corresponding amino acid found in NRC4 and screened these NRC2 variants for susceptibility to SS15 inhibition in cell death assays. This revealed two variants, NRC2$^{E316P}$ and NRC2$^{D317K}$, which triggered cell death when activated by Rx/CP and were no longer inhibited by SS15 (Fig. 3C and figs. S6 and S7). We also tested all 13 single amino acid mutants for association with SS15 by in planta co-immunoprecipitation and found that NRC2$^{E316P}$ and NRC2$^{D317K}$ exhibited reduced association with SS15 relative to NRC2 (Fig. 3D and fig. S6), which is in line with the observation that SS15 is not able to suppress these variants (Fig. 3C). All other NRC2 variants generated were indistinguishable from NRC2 in terms of their capacity to trigger HR when activated by Rx/CP and were all suppressed by SS15, except for NRC2$^{E324V}$, which did not accumulate in planta (fig. S6). We conclude that the E316 and D317 residues are critical for SS15-mediated inhibition of NRC2 and that mutating these residues to their equivalent amino acid in NRC4 allows Rx/CP-activated NRC2 to evade SS15 association and inhibition.

### A bioengineered NRC2$^{D317K}$ variant resurrects the activity of multiple NRC2-dependent sensors in the presence of SS15

We next tested whether these two SS15-evading variants of NRC2 could restore the functionality of NRC2-dependent sensor NLRs that are suppressed by the parasite effector. We tested this by performing complementation assays with NRC2$^{E316P}$ and NRC2$^{D317K}$ in *nrc2/3/4* CRISPR KO *N. benthamiana* plants. We activated the NRC2 variants with a panel of agronomically important sensor NLRs mediating resistance to diverse pathogens, including the potato cyst nematode R protein Gpa2 (an allele of Rx), as well as other well-characterized oomycete and bacterial resistance proteins. NRC2$^{D317K}$ evaded SS15 inhibition with all tested sensor NLRs restoring their capacity to activate immune signaling (Fig. 4A and figs. S8 and S9). In contrast, NRC2$^{E316P}$ could evade SS15 suppression when activated by Rx, but not when activated by other sensors. We therefore selected NRC2$^{D317K}$ for follow-up biochemical studies, using BN-PAGE–based assays. Unlike NRC2, activated NRC2$^{D317K}$ oligomerized even in the presence of SS15 and did not form an in vivo complex with the inhibitor (Fig. 4B). We conclude that NRC2$^{D317K}$ can fully evade SS15-mediated immune suppression, retaining the capacity to oligomerize and mediate cell death when activated by multiple agronomically important sensor NLRs.

## DISCUSSION

Our study reveals how a parasite effector has evolved as an inhibitor of a helper NLR by directly binding its NB-ARC domain to prevent resistosome formation and immune signaling. By binding and immobilizing a critical hinge loop in the HD1 region of the NB-ARC, SS15 restricts movement of the NB domain relative to the HD1 and WHD domains, preventing immune receptor activation. While SS15 can bind and inhibit NRC2, it cannot bind or inhibit the NRC2 paralog NRC4. We exploited NRC4's resilience to SS15 inhibition by making chimeric NRC2-NRC4 variants that, together

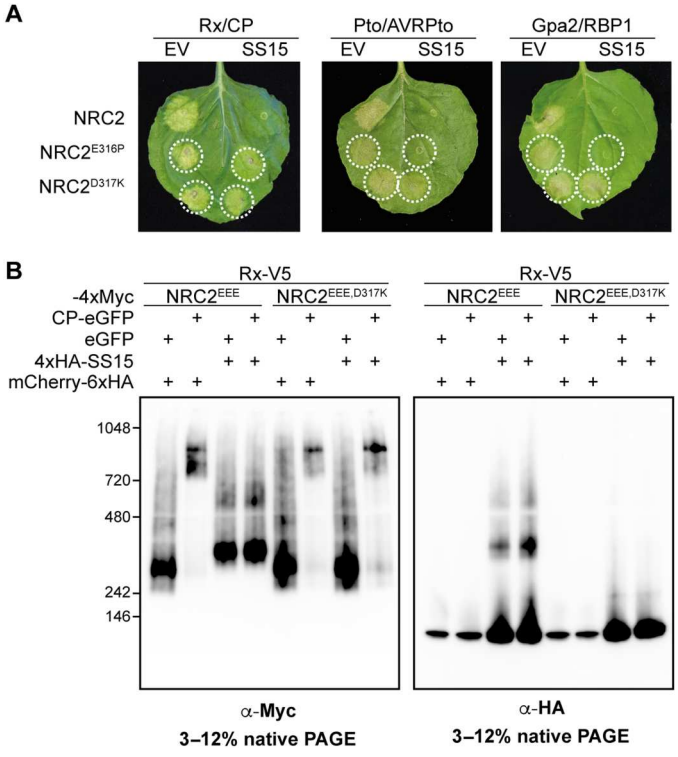


**Fig. 4. NRC2$^{D317K}$ helper restores immune signaling of multiple disease resistance genes in the presence of the effector SS15.** (**A**) Photo of representative leaves from *N. benthamiana nrc2/3/4* KO plants showing HR after coexpression of Rx/CP, Pto/AVRPto, or Gpa2/RBP1 together with NRC2, NRC2$^{E316P}$, or NRC2$^{D317K}$ in the absence or presence of SS15. The experiment consisted of three biological replicates. A quantitative analysis of HR phenotypes can be found in fig. S8. (**B**) BN-PAGE assays with inactive and active Rx together with NRC2 or NRC2$^{D317K}$, in the absence or presence of SS15. C-terminally V5-tagged Rx and C-terminally 4xMyc-tagged NRC2$^{EEE}$ or NRC2$^{EEE,D317K}$ were coexpressed with either free GFP or C-terminally GFP-tagged PVX CP. These effector-sensor-helper combinations were coexpressed together with a 6xHA-mCherry fusion protein or with N-terminally 4xHA-tagged SS15. Total protein extracts were run in parallel on blue native and denaturing PAGE assays and immunoblotted with the appropriate antisera labeled below. Approximate molecular weights (in kilodaltons) of the proteins are shown on the left. Corresponding SDS-PAGE blots can be found in fig. S9. The experiment was repeated three times with similar results.

with structural information, helped us identify the inhibitor binding interface. Mutational studies of this interface allowed us to generate A amino acid variant of NRC2 (NRC2$^{D317K}$) that evades SS15 inhibition without compromising receptor signaling capacity. This NRC2$^{D317K}$ variant can now support signaling by any NRC2-dependent sensor even in the presence of SS15.

In the future, we will address the conservation of the NRC-SS15 interface across NLR proteins. In particular, understanding the degree of conservation of the NRC-SS15 interface across solanaceous NRCs, notably at position 317, can be of great use. This will allow us to determine whether substitutions analogous to NRC2$^{D317K}$ can be effective at evading SS15 suppression when deployed in NRCs from different solanaceous crop species. Moreover, evolutionary analyses coupled with ancestral sequence reconstruction may enable reconstructing the evolutionary trajectory of the NRC-SS15 interface to gain a deeper understanding of the coevolutionary dynamics between NLRs and their pathogen inhibitors.

The existence of plant parasite–secreted NLR inhibitors suggests that suppressed resistance genes may occur in crop genomes. Leveraging the approach detailed in this study, it may be possible to resurrect cryptic or defeated resistance proteins to enhance disease resistance. Moreover, considering that multiple sensors can signal through the same downstream helper, applying this approach to helper NLRs holds potential to simultaneously resurrect multiple upstream sensor NLRs. The single amino acid NRC2 variants we identified could be generated in locus using gene editing technologies in agronomically important crop species, making deployment of this technology viable in countries where transgenic approaches are not feasible. Our work describes a potential approach to achieve robust immunity by engineering NLRs that avoid parasite suppression. This could, in theory, be applied to other plant, metazoan, or even prokaryotic NLR immune receptors that are directly targeted by parasite effectors (*12*, *15*, *16*, *24*). Combined with recent advances in NLR engineering to bioengineer pathogen recognition specificities (*18*, *28*), this technology holds the potential to facilitate synthetic disease resistance breeding.

## MATERIALS AND METHODS

### Plant growth conditions

Wild-type and *nrc2/3/4* CRISPR mutant *N. benthamiana* lines were grown in a controlled environment growth chamber with a temperature range of 22° to 25°C, humidity of 45 to 65%, and a 16-hour light/8-hour dark cycle.

### Plasmid construction

We used the Golden Gate Modular Cloning (MoClo) kit (*29*) and the MoClo plants part kit (*30*) for cloning. All vectors used were generated with these kits unless otherwise stated. Cloning design and sequence analysis were done using Geneious Prime (v2021.2.2; www.geneious.com). Plasmid construction is described in more detail in table S1.

### Cell death assays by agroinfiltration

Proteins of interest were transiently expressed in *N. benthamiana* according to previously described methods (*4*). Briefly, leaves from 4- to 5-week-old plants were infiltrated with suspensions of *Agrobacterium tumefaciens* GV3101 pM90 strains transformed with expression vectors coding for different proteins indicated. The final $OD_{600}$ (optical density at 600 nm) of all *A. tumefaciens* suspensions were adjusted in infiltration buffer [10 mM MES, 10 mM $MgCl_2$, and 150 μM acetosyringone (pH 5.6)]. The final $OD_{600}$ used for each construct is described in table S2.

### Extraction of total proteins for BN-PAGE and SDS-PAGE assays

Four- to 5-week-old *N. benthamiana* plants were agroinfiltrated as described above with constructs of interest, and leaf tissue was collected 3 days after agroinfiltration for NRC2 and 2 days after agroinfiltration for NRC4. The final $OD_{600}$ used for each construct is described in table S2. BN-PAGE was performed using the bis-tris NativePAGE system (Invitrogen) according to the manufacturer's instructions, as described previously (*4*). Leaf tissue was ground using a Geno/Grinder tissue homogenizer. For NRC2, GTMN

extraction buffer was used [10% glycerol, 50 mM tris-HCl (pH 7.5), 5 mM $MgCl_2$, and 50 mM NaCl] supplemented with 10 mM dithiothreitol (DTT), 1× protease inhibitor cocktail (Sigma-Aldrich), and 0.2% NP-40 substitute (Sigma-Aldrich). For NRC4, GHMN buffer [10% glycerol, 50 mM Hepes (pH 7.4), 5 mM $MgCl_2$, and 50 mM NaCl] buffer supplemented with 10 mM DTT, 1× protease inhibitor cocktail (Sigma-Aldrich), and 1% digitonin (Sigma-Aldrich) was used for extraction. Samples were incubated in extraction buffer on ice for 10 min with short vortex mixing every 2 min. Following incubation, samples were centrifuged at 5000*g* for 15 min, and the supernatant was used for BN-PAGE and SDS-PAGE assays.

### BN-PAGE assays

For BN-PAGE, samples extracted as detailed above were diluted as per the manufacturer's instructions by adding NativePAGE 5% G-250 sample additive, 4× sample buffer, and water. After dilution, samples were loaded and run on NativePAGE 3 to 12% bis-tris gels alongside either NativeMark unstained protein standard (Invitrogen) or SERVA Native Marker (SERVA). The proteins were then transferred to polyvinylidene difluoride membranes using the NuPAGE Transfer Buffer using a Trans-Blot Turbo transfer system (Bio-Rad) as per the manufacturer's instructions. Proteins were fixed to the membranes by incubating with 8% acetic acid for 15 min, washed with water, and left to dry. Membranes were subsequently reactivated with methanol to correctly visualize the unstained native protein marker. Membranes were immunoblotted as described below.

### SDS-PAGE assays

For SDS-PAGE, samples were diluted in SDS loading dye and denatured at 72°C for 10 min. Denatured samples were spun down at 5000*g* for 3 min, and the supernatant was run on Bio-Rad 4 to 20% Mini-PROTEAN TGX gels alongside a PageRuler Plus prestained protein ladder (Thermo Fisher Scientific). The proteins were then transferred to polyvinylidene difluoride membranes using the Trans-Blot Turbo transfer buffer using a Trans-Blot Turbo transfer system (Bio-Rad) as per the manufacturer's instructions. Membranes were immunoblotted as described below.

### Immunoblotting and detection of BN-PAGE and SDS-PAGE assays

Blotted membranes were blocked with 5% milk in tris-buffered saline and 0.01% Tween 20 (TBS-T) for an hour at room temperature and subsequently incubated with desired antibodies at 4°C overnight. Antibodies used were anti-GFP (B-2) horseradish peroxidase (HRP) (Santa Cruz Biotechnology), anti-hemagglutinin (HA) (3F10) HRP (Roche), anti-Myc (9E10) HRP (Roche), and anti-V5 (V2260) HRP (Roche), all used in a 1:5000 dilution in 5% milk in TBS-T. To visualize proteins, we used Pierce ECL Western (32106, Thermo Fisher Scientific), supplementing with up to 50% SuperSignal West Femto Maximum Sensitivity Substrate (34095, Thermo Fisher Scientific) when necessary. Membrane imaging was carried out with an ImageQuant LAS 4000 or an ImageQuant 800 luminescent imager (GE Healthcare Life Sciences, Piscataway, NJ). Rubisco loading control was stained using Ponceau S (Sigma-Aldrich).

### Co-immunoprecipitation assays

Co-immunoprecipitation assays were performed as described previously (*15*). Total soluble protein was extracted as described above from leaves of *N. benthamiana* 3 days after agroinfiltration using the GTEN buffer [10% glycerol, 25 mM tris-HCl (pH 7.5), 1 mM EDTA, and 150 mM NaCl] supplemented with 2% (w/v) polyvinylpolypyrrolidone (PVPP), 10 mM DTT, and 1× protease inhibitor cocktail (Sigma-Aldrich), as well as 0.3% IGEPAL (Sigma-Aldrich). $OD_{600}$ used can be found in table S2. Protein extracts were filtered using Minisart 0.45-µm filters (Sartorius Stedim Biotech, Goettingen, Germany). Part of the extract was set aside before immunoprecipitation and used for SDS-PAGE as described above. These were the inputs. A total of 1.4 ml of the remaining filtered total protein extract was mixed with 30 µl of anti–c-Myc agarose beads (A7470, Sigma-Aldrich) and incubated end over end for 90 min at 4°C. Beads were washed five times with immunoprecipitation wash buffer [GTEN extraction buffer with 0.3% (v/v) IGEPAL (Sigma-Aldrich)] and resuspended in 60 µl of SDS loading dye. Proteins were eluted from beads by heating for 10 min at 72°C. Immunoprecipitated samples were used for SDS-PAGE and immunoblotted as described above and compared to the inputs.

### Confocal microscopy

Three- to 4-week-old plants were agroinfiltrated as described above with constructs of interest. The final $OD_{600}$ used for each construct is described in table S2. Leaf tissue was prepared for imaging by sectioning of the desired area surrounding an infiltration spot using a cork borer size 4 and was mounted, live, in wells containing $dH_2O$ made in Carolina Observation Gel to enable diffusion of gasses. The abaxial of the leaf tissue was imaged using a Leica SP8 with 40× water immersion objective. Laser excitations for fluorescent proteins were used as described previously (*31*), namely, 488 nm (argon) for GFP, 561/594 nm (diode) for red fluorescent protein, and 405 nm (diode) for blue fluorescent protein.

### Membrane enrichment assays

Membrane enrichment was carried out by slightly modifying a previously described protocol (*32*). Briefly, the leaf material was ground to fine powder using liquid nitrogen and 2× volume of extraction buffer was added. Extraction buffer consisted of 0.81 M sucrose, 5% (v/v) glycerol, 10 mM EDTA, 10 mM EGTA, 5 mM KCl, and 100 mM tris-HCl (pH 7.5) supplemented with 5 mM DTT, 1% Sigma-Aldrich plant protease inhibitor cocktail, 1 mM phenylmethylsulfonyl fluoride, and 0.5% PVPP. After addition of the buffer, the samples were vortexed for a minute, and the cell debris was cleared out by two subsequent centrifugation steps at 1000*g* for 5 min. The supernatant was diluted 1:1 using distilled water, and an aliquot of the supernatant was separated as the total fraction (*T*). The remaining supernatant (200 to 300 µl) was further centrifuged at 21,000*g* for 90 min at 4°C. This centrifugation yielded the supernatant (soluble fraction, *S*) and membrane-enriched pellet (membrane fraction, *M*). After separating the soluble fraction, the pellet was resuspended in diluted extraction buffer (without PVPP). All the fractions were diluted with SDS loading dye, and proteins were denatured by incubating at 50°C for 15 min. Western blotting was performed as previously described following SDS-PAGE. Endogenous plasma membrane ATPase was detected using an anti-H + ATPase (AS07 260) antibody (Agrisera) as a marker to show the success of membrane enrichment.

### Heterologous protein production and purification from *Escherichia coli*

Heterologous production and purification of SS15 was performed as previously described (*15*). Recombinant SS15 protein (lacking signal peptide) was expressed by cloning in pOPIN-S3C plasmid, with an N-terminal tandem 6xHis-SUMO followed by a 3C protease cleavage site. pOPIN-S3C:SS15 was transformed into *Escherichia coli* SHuffle cells. Eight liters of these cells were grown at 30°C in autoinduction medium (*33*) to an $OD_{600}$ of 0.6 to 0.8 followed by overnight incubation at 18°C and harvested by centrifugation. Pelleted cells were resuspended in 50 mM tris-HCl (pH 8), 500 mM NaCl, 50 mM glycine, 5% (v/v) glycerol, and 20 mM imidazole (buffer A) supplemented with cOmplete EDTA-free protease inhibitor tablets (Roche) and lysed by sonication. The clarified cell lysate was applied to a $Ni^{2+}$-NTA column connected to an AKTA pure system. 6xHis-SUMO-SS15 was step eluted with elution buffer (buffer A with 500 mM imidazole) and directly injected onto a Superdex 200 26/600 gel filtration column pre-equilibrated with buffer B [20 mM Hepes (pH 7.5) and 150 mM NaCl]. The fractions containing 6xHis-SUMO-SS15 were pooled, and the N-terminal 6xHis-SUMO tag was cleaved by addition of 3C protease (10 μg/mg of fusion protein), incubating overnight at 4°C. Cleaved SS15 was further purified using a $Ni^{2+}$-NTA column, this time collecting the flow-through to separate the cleaved tag from the SS15 protein. Untagged SS15 was further purified by another round of gel filtration as described above. The concentration of protein was judged by absorbance at 280 nm (using a calculated molar extinction coefficient of 35,920 $M^{-1}$ $cm^{-1}$ for SS15).

Heterologous production and purification of $SlNRC1^{NB\text{-}ARC}$ was performed as previously described (*34*). Recombinant $SlNRC1^{NB\text{-}ARC}$ protein was also expressed cloning in pOPIN-S3C plasmid as described above. pOPIN-S3C:$SlNRC1^{NB\text{-}ARC}$ was transformed into *E. coli* Lemo21 (DE3) cells. Eight liters of these cells were grown at 37°C in autoinduction medium (*33*) to an $OD_{600}$ of 0.6 to 0.8 followed by overnight incubation at 18°C and harvested by centrifugation. Pelleted cells were resuspended in 50 mM tris-HCl (pH 8), 500 mM NaCl, 50 mM glycine, 5% (v/v) glycerol, and 20 mM imidazole (buffer A) supplemented with cOmplete EDTA-free protease inhibitor tablets (Roche) and lysed by sonication. The clarified cell lysate was applied to a $Ni^{2+}$-NTA column connected to an AKTA pure system. 6xHis-SUMO-$SlNRC1^{NB\text{-}ARC}$ was step eluted with elution buffer (buffer A with 500 mM imidazole) and directly injected onto a Superdex 200 26/600 gel filtration column pre-equilibrated with buffer B [20 mM Hepes (pH 7.5) and 150 mM NaCl]. The fractions containing 6xHis-SUMO-$SlNRC1^{NB\text{-}ARC}$ were pooled, and the N-terminal 6xHis-SUMO tag was cleaved by addition of 3C protease (10 μg/mg of fusion protein), incubating overnight at 4°C. Cleaved $SlNRC1^{NB\text{-}ARC}$ was further purified using a $Ni^{2+}$-NTA column, this time collecting the flow-through to separate the cleaved tag from the $SlNRC1^{NB\text{-}ARC}$ protein. Untagged $SlNRC1^{NB\text{-}ARC}$ was further purified by another round of gel filtration as described above. The concentration of protein was judged by absorbance at 280 nm (using a calculated molar extinction coefficient of 63,370 $M^{-1}$ $cm^{-1}$ for $SlNRC1^{NB\text{-}ARC}$).

To obtain $SlNRC1^{NB\text{-}ARC}$ in complex with SS15, both proteins were incubated in a 1:1 molar ratio overnight at 4°C and subjected to gel filtration on a Superdex 200 26/600 gel filtration column as described above. The fractions containing $SlNRC1^{NB\text{-}ARC}$ in complex with SS15 were pooled, concentrated to 10 to 15 mg/ml, and subsequently used for crystallization screens.

### Crystallization, data collection, and structure solution

Crystallization screens were performed at 18°C using the sitting-drop vapor diffusion technique. Drops composed of 0.3 μl of protein solution and 0.3 μl of reservoir solution were set up in MRC 96-well crystallization plates (Molecular Dimensions), which were dispensed using an Oryx Nano or an Oryx8 robot (Douglas Instruments). Crystal growth was monitored using a Minstrel Desktop Crystal Imaging System (Rikagu). Suitable crystals grew after 72 hours in a Morpheus screen crystallization condition containing 0.1 M MES buffer (pH 6.5), 10% (w/v) PEG-8000 (polyethylene glycol, molecular weight 8000), and 20% (v/v) ethylene glycol (Molecular Dimensions) and were harvested by flash-cooling in liquid nitrogen using LithoLoops (Molecular Dimensions). X-ray diffraction data were collected at the Diamond Light Source (Didcot, UK) on beamline I03 using an Eiger2 XE 16M pixel array detector (Dectris) with crystals maintained at 100 K by a Cryojet cryocooler (Oxford Instruments).

X-ray data were integrated and scaled using X-ray Detection Software (XDS) (*35*), as implemented through the XIA2 (*36*) pipeline, and then merged using AIMLESS (*37*), via the CCP4i2 graphical user interface (*38*). The $NRC1^{NB\text{-}ARC}$-SS15 complex crystallized in space group $P6_1$ with cell parameters $a = b = 128.6$ and $c = 170.7$ Å, and the Most Unexceptional crystal yielded diffraction data to 4.5 Å resolution (see table S3 for a summary of data collection and refinement statistics). Given the small size of the dataset, we assigned 10% of the data (883 unique reflections) for the $R_{free}$ calculation, to give a more statistically meaningful metric. The crystal structure of $NRC1^{NB\text{-}ARC}$ alone was already available [Protein Data Bank (PDB) 6S2P], but there was no experimentally determined structure for SS15. Thus, we made use of AlphaFold2 (AF2) multimer (*39*), as implemented through ColabFold (*40*) to generate structural predictions for the complex. There was very good sequence coverage for both proteins, and the five independent models of the individual components were closely similar. The predicted local distance difference test (pLDDT) scores were generally good (e.g., averages of 82 and 75 for $NRC1^{NB\text{-}ARC}$ and SS15 models, respectively, from the rank 1 predictions). However, the relative placement of the two components varied across the five models, and the corresponding predicted aligned error (PAE) scores indicated very low confidence in these predictions. A comparison of the five $NRC1^{NB\text{-}ARC}$ models with the known crystal structure showed a good agreement (e.g., superposition of the rank 1 model gave a root mean square deviation of 1.77 Å). Given that the AF2 model provided starting coordinates for several loops missing from the crystal structure, we decided to use this model in molecular replacement. Templates for both components were prepared using the "Process Predicted Models" CCP4i2 task, which removed low-confidence regions (based on pLDDT) and converted the pLDDT scores in the *B* factor field of the PDB coordinate files to pseudo *B* factors. Analysis of the likely composition of the asymmetric unit (ASU) suggested that it contained two copies of each component, giving an estimated solvent content of ~67%. Phaser (*41*) was able to place the four chains within the ASU, although the second SS15 domain required manual repositioning with respect to its neighboring NRC1 domain to avoid a number of clashes and improve the fit to the density. This was achieved using COOT (*42*) and guided by the arrangement of

the other NRC1-SS15 complex (fig. S4). The structure was then subjected to jelly body refinement in REFMAC5 (*43*) using ProSMART restraints (*44*) generated from the AF2 models, giving $R_{work}$ and $R_{free}$ values of 0.357 and 0.401, respectively, to a 4.5-Å resolution.

Now, it was possible to generate more complete models for the components by superposing the original unprocessed AF2 models and trimming these with reference to the improved electron density. Furthermore, a substantial region of positive difference density was present at the cores of both NRC1 domains, which corresponded to the adenosine diphosphate (ADP) in the crystal structure; thus, we incorporated ADP into the model. Because of the low resolution of the dataset, only very limited rebuilding was possible in COOT, where Geman-McClure and Ramachandran restraints were used to maintain good stereochemical parameters. After several cycles of restrained refinement in REFMAC5 and editing in COOT, a reasonable model was obtained with $R_{work}$ and $R_{free}$ values of 0.258 and 0.298, respectively. However, there remained a region of positive difference density near the N termini of both SS15 domains that we could not adequately explain. At this point, we reran the AF2 multimer predictions, but this time with one copy of the complex taken from the crystal structure as a reference template. Although these computational predictions did not produce complexes that were consistent with the x-ray data, and the models for the individual components did not appear to be noticeably improved based on pLDDT scores, we used them as starting points to rebuild the x-ray structure.

Notably, for several models, the N-terminal region of SS15 adopted conformations that partially accounted for the region of positive difference electron density, and this could be improved by careful rebuilding and refinement. This "AlphaFold recycling" procedure was repeated a further two times before finalizing the structure, which included residues 153 to 494 for SlNRC1 (numbered with respect to the full-length protein) and residues 18 to 223 for SS15, where residues 33 to 43 in both copies of the latter formed α helices that occupied the regions of positive difference density observed earlier. For the last refinement in REFMAC5, the following options were used: ProSMART restraints generated from the latest AF2 models, overall *B* factor refinement with translation/libration/screw (TLS) restraints (where each protein chain was treated as a separate domain), and noncrystallographic symmetry restraints. The final model gave $R_{work}$ and $R_{free}$ values of 0.237 and 0.275, respectively, to a 4.5-Å resolution (see table S3 for a summary of refinement statistics). All structural figures were prepared using ChimeraX (*45*) and PyMOL (*46*).

## Supplementary Materials

**This PDF file includes:**
Figs. S1 to S9
Legends for tables S1 and S2
Table S3
Legend for movie S1
References

**Other Supplementary Material for this manuscript includes the following:**
Tables S1 and S2
Movie S1

## REFERENCES AND NOTES


1. J. D. Jones, R. E. Vance, J. L. Dangl, Intracellular innate immune surveillance devices in plants and animals. *Science* **354**, aaf6395 (2016).
2. Z. Duxbury, C.-H. Wu, P. Ding, A comparative overview of the intracellular guardians of plants and animals: NLRs in innate immunity and beyond. *Annu. Rev. Plant Biol.* **72**, 155–184 (2021).
3. J. Wang, M. Hu, J. Wang, J. Qi, Z. Han, G. Wang, Y. Qi, H. W. Wang, J. M. Zhou, J. Chai, Reconstitution and structure of a plant NLR resistosome conferring immunity. *Science* **364**, eaav5870 (2019).
4. M. P. Contreras, H. Pai, Y. Tumtas, C. Duggan, E. L. H. Yuen, A. V. Cruces, J. Kourelis, H.-K. Ahn, K.-T. Lee, C.-H. Wu, T. O. Bozkurt, L. Derevnina, S. Kamoun, Sensor NLR immune proteins activate oligomerization of their NRC helpers in response to plant pathogens. *The EMBO Journal* **42**, e111519 (2023).
5. H.-K. Ahn, X. Lin, A. C. Olave-Achury, L. Derevnina, M. P. Contreras, J. Kourelis, S. Kamoun, J. D. G. Jones, Effector-dependent activation and oligomerization of plant NRC class helper NLRs by sensor NLR immune receptors Rpi-amr3 and Rpi-amr1. *The EMBO Journal* **42**, e111484 (2023).
6. A. Förderer, E. Li, A. W. Lawson, Y. Deng, Y. Sun, E. Logemann, X. Zhang, J. Wen, Z. Han, J. Chang, Y. Chen, P. Schulze-Lefert, J. Chai, A wheat resistosome defines common principles of immune receptor channels. *Nature* **610**, 532-539 (2022).
7. R. Martin, T. Qi, H. Zhang, F. Liu, M. King, C. Toth, E. Nogales, B. J. Staskawicz, Structure of the activated ROQ1 resistosome directly recognizing the pathogen effector XopQ. *Science* **370**, eabd9993 (2020).
8. I. V. Hochheiser, M. Pilsl, G. Hagelueken, J. Moecking, M. Marleaux, R. Brinkschulte, E. Latz, C. Engel, M. Geyer, Structure of the NLRP3 decamer bound to the cytokine release inhibitor CRID3. *Nature* **604**, 184–189 (2022).
9. Z. Hu, Q. Zhou, C. Zhang, S. Fan, W. Cheng, Y. Zhao, F. Shao, H. W. Wang, S. F. Sui, J. Chai, Structural and biochemical basis for induced self-propagation of NLRC4. *Science* **350**, 399–404 (2015).
10. Z. Duxbury, S. Wang, C. I. MacKenzie, J. L. Tenthorey, X. Zhang, S. U. Huh, L. Hu, L. Hill, P. M. Ngou, P. Ding, J. Chen, Y. Ma, H. Guo, B. Castel, P. N. Moschou, M. Bernoux, P. N. Dodds, R. E. Vance, J. D. G. Jones, Induced proximity of a TIR signaling domain on a plant-mammalian NLR chimera activates defense in plants. *Proc. Natl. Acad. Sci. U.S.A.* **117**, 18832–18839 (2020).
11. B. P. M. Ngou, P. Ding, J. D. Jones, Thirty years of resistance: Zig-zag through the plant immune system. *Plant Cell* **34**, 1447–1478 (2022).
12. L. A. Gao, M. E. Wilkinson, J. Strecker, K. S. Makarova, R. K. Macrae, E. V. Koonin, F. Zhang, Prokaryotic innate immunity through pattern recognition of conserved viral proteins. *Science* **377**, eabm4096 (2022).
13. C.-H. Wu, L. Derevnina, S. Kamoun, Receptor networks underpin plant immunity. *Science* **360**, 1300–1301 (2018).
14. L. D. Cunha, J. M. Ribeiro, T. D. Fernandes, L. M. Massis, C. A. Khoo, J. H. Moffatt, H. J. Newton, C. R. Roy, D. S. Zamboni, Inhibition of inflammasome activation by *Coxiella burnetii* type IV secretion system effector IcaA. *Nat. Commun.* **6**, 10205 (2015).
15. L. Derevnina, M. P. Contreras, H. Adachi, J. Upson, A. Vergara Cruces, R. Xie, J. Skłenar, F. L. H. Menke, S. T. Mugford, D. MacLean, W. Ma, S. A. Hogenhout, A. Goverse, A. Maqbool, C. H. Wu, S. Kamoun, Plant pathogens convergently evolved to counteract redundant nodes of an NLR immune receptor network. *PLOS Biol.* **19**, e3001136 (2021).
16. H. Yen, N. Sugimoto, T. Tobe, Enteropathogenic Escherichia coli uses NleA to inhibit NLRP3 inflammasome activation. *PLOS Pathog.* **11**, e1005121 (2015).
17. Q. Chai, S. Yu, Y. Zhong, Z. Lu, C. Qiu, Y. Yu, X. Zhang, Y. Zhang, Z. Lei, L. Qiang, B. X. Li, Y. Pang, X. B. Qiu, J. Wang, C. H. Liu, A bacterial phospholipid phosphatase inhibits host pyroptosis by hijacking ubiquitin. *Science* **378**, eabq0132 (2022).
18. C. Marchal, H. Pai, S. Kamoun, J. Kourelis, Emerging principles in the design of bioengineered made-to-order plant immune receptors. *Curr. Opin. Plant Biol.* **70**, 102311 (2022).
19. J. Kourelis, T. Sakai, H. Adachi, S. Kamoun, RefPlantNLR is a comprehensive collection of experimentally validated plant disease resistance proteins from the NLR family. *PLOS Biol.* **19**, e3001124 (2021).
20. H. Adachi, L. Derevnina, S. Kamoun, NLR singletons, pairs, and networks: Evolution, assembly, and regulation of the intracellular immunoreceptor circuitry of plants. *Curr. Opin. Plant Biol.* **50**, 121–131 (2019).
21. C.-H. Wu, A. Abd-el-Haliem, T. O. Bozkurt, K. Belhaj, R. Terauchi, J. H. Vossen, S. Kamoun, NLR network mediates immunity to diverse plant pathogens. *Proc. Natl. Acad. Sci. U.S.A.* **114**, 8113–8118 (2017).
22. C. N. LaRock, B. T. Cookson, The Yersinia virulence effector YopM binds caspase-1 to arrest inflammasome assembly and processing. *Cell Host Microbe* **12**, 799–805 (2012).
23. H. Chen, D. Yang, F. Han, J. Tan, L. Zhang, J. Xiao, Y. Zhang, Q. Liu, The bacterial T6SS effector EvpP prevents NLRP3 inflammasome activation by inhibiting the $Ca^{2+}$-dependent MAPK-Jnk pathway. *Cell Host Microbe* **21**, 47–58 (2017).

24. H. S. Karki, S. Abdullah, Y. Chen, D. A. Halterman, Natural genetic diversity in the potato resistance gene RB confers suppression avoidance from Phytophthora effector IPI-O4. *Mol. Plant Microbe Interact.* **34**, 1048–1056 (2021).
25. H. Adachi, M. P. Contreras, A. Harant, C. H. Wu, L. Derevnina, T. Sakai, C. Duggan, E. Moratto, T. O. Bozkurt, A. Maqbool, J. Win, S. Kamoun, An N-terminal motif in NLR immune receptors is functionally conserved across distantly related plant species. *eLife* **8**, e49956 (2019).
26. J. Kourelis, M. P. Contreras, A. Harant, H. Pai, D. Lüdke, H. Adachi, L. Derevnina, C.-H. Wu, S. Kamoun, The helper NLR immune protein NRC3 mediates the hypersensitive cell death caused by the cell-surface receptor Cf-4. *PLoS Genetics* **18**, e1010414 (2022).
27. J. Wang, J. Wang, M. Hu, S. Wu, J. Qi, G. Wang, Z. Han, Y. Qi, N. Gao, H. W. Wang, J. M. Zhou, J. Chai, Ligand-triggered allosteric ADP release primes a plant NLR complex. *Science* **364**, eaav5868 (2019).
28. J. Kourelis, C. Marchal, A. Posbeyikian, A. Harant, S. Kamoun, NLR immune receptor-nanobody fusions confer plant disease resistance. *Science* **379**, 934–939 (2023).
29. E. Weber, C. Engler, R. Gruetzner, S. Werner, S. Marillonnet, A modular cloning system for standardized assembly of multigene constructs. *PLOS ONE* **6**, e16765 (2011).
30. C. Engler, M. Youles, R. Gruetzner, T. M. Ehnert, S. Werner, J. D. G. Jones, N. J. Patron, S. Marillonnet, A golden gate modular cloning toolbox for plants. *ACS Synth. Biol.* **3**, 839–843 (2014).
31. C. Duggan, E. Moratto, Z. Savage, E. Hamilton, H. Adachi, C. H. Wu, A. Y. Leary, Y. Tumtas, S. M. Rothery, A. Maqbool, S. Nohut, T. R. Martin, S. Kamoun, T. O. Bozkurt, Dynamic localization of a helper NLR at the plant–pathogen interface underpins pathogen recognition. *Proc. Natl. Acad. Sci. U.S.A.* **118**, e2104997118 (2021).
32. L. Abas, C. Luschnig, Maximum yields of microsomal-type membranes from small amounts of plant material without requiring ultracentrifugation. *Anal. Biochem.* **401**, 217–227 (2010).
33. F. W. Studier, Protein production by auto-induction in high-density shaking cultures. *Protein Expr. Purif.* **41**, 207–234 (2005).
34. J. F. Steele, R. K. Hughes, M. J. Banfield, Structural and biochemical studies of an NB-ARC domain from a plant NLR immune receptor. *PLOS ONE* **14**, e0221226 (2019).
35. W. Kabsch, XDS. *Acta Crystallogr. D Biol. Crystallogr.* **66**, 125–132 (2010).
36. G. Winter, xia2: An expert system for macromolecular crystallography data reduction. *J. Appl. Cryst.* **43**, 186–190 (2010).
37. P. R. Evans, G. N. Murshudov, How good are my data and what is the resolution? *Acta Crystallogr. D Biol. Crystallogr.* **69**, 1204–1214 (2013).
38. M. D. Winn, An overview of the CCP4 project in protein crystallography: An example of a collaborative project. *J. Synchrotron Radiat.* **10**, 23–25 (2003).
39. R. Evans, M. O'Neil, A. Pritzel, N. Antropova, A. Senior, T. Green, A. Žídek, R. Bates, S. Blackwell, J. Yim, O. Ronneberger, S. Bodenstein, M. Zielinski, A. Bridgland, A. Potapenko, A. Cowie, K. Tunyasuvunakool, R. Jain, E. Clancy, P. Kohli, J. Jumper, D. Hassabis, Protein complex prediction with AlphaFold-Multimer. bioRxiv 2021.10.04.463034 [Preprint]. 10 March 2022. https://doi.org/10.1101/2021.10.04.463034.
40. M. Mirdita, K. Schütze, Y. Moriwaki, L. Heo, S. Ovchinnikov, M. Steinegger, ColabFold: Making protein folding accessible to all. *Nat. Methods* **19**, 679–682 (2022).
41. A. J. McCoy, R. W. Grosse-Kunstleve, P. D. Adams, M. D. Winn, L. C. Storoni, R. J. Read, Phaser crystallographic software. *J. Appl. Cryst.* **40**, 658–674 (2007).
42. P. Emsley, B. Lohkamp, W. G. Scott, K. Cowtan, Features and development of Coot. *Acta Crystallogr. D Biol. Crystallogr.* **66**, 486–501 (2010).
43. G. N. Murshudov, P. Skubák, A. A. Lebedev, N. S. Pannu, R. A. Steiner, R. A. Nicholls, M. D. Winn, F. Long, A. A. Vagin, REFMAC5 for the refinement of macromolecular crystal structures. *Acta Crystallogr. D Biol. Crystallogr.* **67**, 355–367 (2011).
44. R. A. Nicholls, M. Fischer, S. McNicholas, G. N. Murshudov, Conformation-independent structural comparison of macromolecules with ProSMART. *Acta Crystallogr. D Biol. Crystallogr.* **70**, 2487–2499 (2014).
45. E. F. Pettersen, T. D. Goddard, C. C. Huang, E. C. Meng, G. S. Couch, T. I. Croll, J. H. Morris, T. E. Ferrin, UCSF ChimeraX: Structure visualization for researchers, educators, and developers. *Protein Sci.* **30**, 70–82 (2021).
46. The PyMOL Molecular Graphics System, Version 1.2r3pre, Schrödinger, LLC.
47. M. E. Segretin, M. Pais, M. Franceschetti, A. Chaparro-Garcia, J. I. B. Bos, M. J. Banfield, S. Kamoun, Single amino acid mutations in the potato immune receptor R3a expand response to Phytophthora effectors. *Mol. Plant Microbe Interact.* **27**, 624–637 (2014).
48.. D. MacLean, Besthr. Zenodo (2019). https://doi.org/10.5281/zenodo.3374507.
49. I. W. Davis, A. Leaver-Fay, V. B. Chen, J. N. Block, G. J. Kapral, X. Wang, L. W. Murray, W. B. Arendall, J. Snoeyink, J. S. Richardson, D. C. Richardson, MolProbity: All-atom contacts and structure validation for proteins and nucleic acids. *Nucleic Acids Res.* **35**, W375–W383 (2007).


**Acknowledgments:** We are very thankful to J. Kourelis, C. Marchal, D. Lüdke, and H.-K. Ahn (The Sainsbury Laboratory, Norwich, UK) for invaluable scientific discussions, ideas, and feedback. We thank J. Mundy for assistance with crystallography experiments. We thank the Diamond Light Source, UK (beamline i03 under proposal MX18565) for access to x-ray data collection facilities. M.P.C. thanks L. Messi for inspiration. We thank all members of the TSL Support Services for their invaluable assistance. **Funding:** The authors received funding from the Gatsby Charitable Foundation (to M.P.C., H.P., M.S., A.T., D.M.L., C.E.M.S., A.H., A.M., C.-H.W., S.K., and L.D.), Biotechnology and Biological Sciences Research Council (BBSRC) BB/P012574 (Plant Health ISP) (to M.P.C., H.P., M.S., A.T., D.M.L., C.E.M.S., A.H., A.M., C.-H.W., S.K., and L.D.), BBSRC BBS/E/J/000PR9795 (Plant Health ISP - Recognition) (to M.P.C., H.P., M.S., A.T., D.M.L., C.E.M.S., A.H., A.M., C.-H.W, S.K., and L.D.), BBSRC BBS/E/J/000PR9796 (Plant Health ISP - Response) (to M.P.C., H.P., M.S., A.T., D.M.L., C.E.M.S., A.H., A.M., C.-H.W., S.K., and L.D.), BBSRC BBS/E/J/000PR9797 (Plant Health ISP – Susceptibility) (to M.P.C., H.P., M.S., A.T., D.M.L., C.E.M.S., A.H., A.M., C.-H.W., S.K., and L.D.), BBSRC BBS/E/J/000PR9798 (Plant Health ISP – Evolution) (to M.P.C., H.P., M.S., A.T., D.M.L., C.E.M.S., A.H., A.M., C.-H.W., S.K., and L.D.), BBSRC BB/V002937/1 (to M.P.C., L.D., and S.K.), BBSRC BB/T006102/1 (to Y.T., C.D., and T.O.B.), BBSRC impact acceleration award BB/X511055/1 (to E.L.H.Y.), Academia Sinica and National Science and Technology Council NSTC-111-2628-B-001-023 (to C.-H.W.), and European Research Council (ERC) 743165 (to S.K.). The funders had no role in the study design, data collection and analysis, decision to publish, or preparation of the manuscript. **Author contributions:** Conceptualization: M.P.C., C.-H.W., S.K., and L.D. Methodology: M.P.C., H.P., M.S., D.M.L., C.E.M.S., A.M., and L.D. Validation: M.P.C., H.P., M.S., Y.T., C.D., E.L.H.Y., and A.H. Formal analysis: M.P.C., H.P., M.S., A.T., D.M.L., Y.T., C.D., C.E.M.S., and L.D. Investigation: M.P.C., H.P., M.S., Y.T., C.D., E.L.H.Y., A.H., A.M., and L.D. Data curation: M.P.C., H.P., M.S., A.T., D.M.L., Y.T., C.D., E.L.H.Y., C.E.M.S., A.M., A.H., and L.D. Visualization: M.P.C., H.P., M.S., A.T., Y.T., C.D., E.L.H.Y., and L.D. Funding acquisition: T.O.B., S.K., and L.D. Project administration: M.P.C., T.O.B., S.K., and L.D. Supervision: M.P.C., T.O.B., S.K., and L.D. Writing—original draft: M.P.C., S.K., and L.D. Writing—review and editing: M.P.C., D.M.L., S.K., and L.D. **Competing interests:** C.D., T.O.B., and S.K. receive funding from industry on NLR biology and cofounded a start-up company (Resurrect Bio Ltd.) on resurrecting disease resistance. M.P.C., S.K., and L.D. have filed patents on NLR biology. M.P.C. and L.D. have received fees from Resurrect Bio Ltd. **Data and materials availability:** All data needed to evaluate the conclusions in the paper are present in the paper and/or the Supplementary Materials. Data relevant to the structure presented in Fig. 3 can be found in PDB 8BV0.

Submitted 20 December 2022
Accepted 30 March 2023
Published 3 May 2023
10.1126/sciadv.adg3861